

Advanced Super Alloys with High Performance for Severe Operation Environment Applications

¹Rong Liu, ²Yinping Ding and ³Kafeel Kamal,

^{1,3}Department of Mechanical & Aerospace Engineering, Carleton University, 1125 Colonel By Drive, Ottawa, Ontario, Canada

²Institute of Laser Advanced Manufacturing, Zhejiang University of Technology, No. 288 Liuhe Road, Hangzhou, China

Abstract: Superalloys display exceptional performance in resisting severe wear and corrosion as well as high-temperature degradation. This paper presents a study on 700 Series Stellite alloys, which are cobalt-based superalloys containing high carbon content (> 1 wt.%) with different levels of molybdenum between 5 wt.% and 18 wt.%. The microstructure, hardness, wear and corrosion resistance, of three 700 series Stellite alloys are investigated using scanning electron microscopy (SEM), X-ray diffraction (XRD), a Rockwell hardness tester, a pin-on-disc tribometer, and immersion and electrochemical methods, respectively. It is shown that these alloys exhibit high hardness and excellent wear resistance. Both carbon and molybdenum contents influence the microstructure of these alloys significantly. The former determines the volume fraction of carbides precipitated in the alloys and the latter governs the amount of Mo-rich carbides and intermetallic compounds formed in the alloys. In the severe corrosive medium – Green Death solution, 700 Series Stellite alloys perform superbly owing to the ability of forming protective oxide film and retaining it on the alloy surface due to high chromium and molybdenum contents.

Keywords: Stellite alloy; Molybdenum; Microstructure; Wear; Corrosion

I. INTRODUCTION

Superalloys possess many unusual properties, for example, high-temperature mechanical performance stability, wear and corrosion resistance in severe operation conditions, owing to unique chemical composition [1]. One family of superalloy, designated as Stellite alloy, is cobalt-based alloys, containing carbon (C), chromium (Cr), tungsten (W) and/or molybdenum (Mo). The balance of these alloying elements in the alloys will provide a variety of properties targeted to meet the needs for particular applications [2]. Carbon is a key element in the design of a Stellite alloy because it governs the volume fraction of carbides precipitated in the alloy. High-C Stellite alloys (1.2 to 3 wt.%) are designed for severe wear resistance, medium-C Stellite alloys (0.5 to 1.2 wt.%) can be for both wear and corrosion resistance, and low-C Stellite alloys (< 0.5 wt.%) are designed more for corrosion and high temperature, but also applicable to wear applications [3].

In terms of the alloying elements present, Stellite alloys can be divided into two main categories: CoCrW system and CoCrMo system [4]. Traditional Stellite alloys are mainly CoCrW system such as the most popular Stellite 6, Stellite 3, etc. [5,6,7], except Stellite 21 which is CoCrMo system but contains very low C content [8]. In recent years, a group of Stellite alloy, which switches the W content for Mo in Stellite alloys [9,10,11] This switch still provides solid solution strengthening, but also expects to improve corrosion performance. The increase in Mo content also changes the type of carbides formed in the alloys [12]. These alloys are designated as 700 series Stellite alloys, for example, low-C Stellite 728, high-C Stellite 706, Stellite 712, Stellite 720. The main difference among these alloys is C and Mo contents since they have similar Cr content. As newly developed alloys, high-C 700 series Stellite alloys are promising replacement of traditional Stellite alloys for the applications where severe wear and corrosion concur. However, these new alloys have been rarely studied and reported in literature [13], in

particular, the corrosion behavior of the alloys has never been investigated, thus the expected beneficial effect of Mo on the corrosion resistance of these alloys is not validated. To this end, the present research attempted to characterize three high-C 700 series Stellite alloys, Stellite 706, Stellite 712, and Stellite 720, with different C and Mo contents. The microstructure, hardness, wear and corrosion performance were investigated using SEM/XRD, pin-on-disc tribometer wear test, electrochemical and immersion methods, respectively. The focus of this research was on the response of these characteristics to the Mo replacement for W in these alloys. The outcome of the research will guide the design and application of advanced Stellite alloys.

II. EXPERIMENT AND METHOD

A. Specimen preparation

The cast Stellite 706, Stellite 712 and Stellite 720 specimens used in this research were provided by Kennametal Stellite Inc. The chemical compositions of the alloys are given in Table 1, showing that these alloys contain the same alloying elements but the contents of C and Mo elements vary among them. Stellite 706 has the least amounts of C and Mo, while Stellite 720 has the most.

Table 1 Chemical compositions (wt.%, Co balance) of the 700 series Stellite alloys

Alloy	Cr	Mo	C	Fe	Ni	Si	Mn
Stellite 706	29	5	1.2	3	3	1.5	1.5
Stellite 712	29	8.5	2	3	3	1.5	1.5
Stellite 720	33	18	2.5	3	3	1.5	1.5

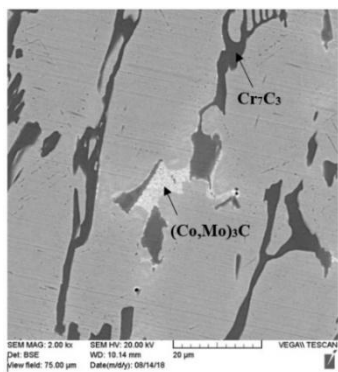
The specimens were ground and polished using a Struers Tegramin-30 automatic grinding/polishing machine, starting with an initial grinding step using 240 grit silicon carbide papers, followed by a polishing step using a MD-Plan (woven polyester) polishing cloth with DiaPro Plan 9 μm diamond suspension, then a final step was taken to achieve a mirror-like surface using a MD-

Dur (satin woven natural silk) polishing cloth with DiaPro Dur 3µm diamond suspension.

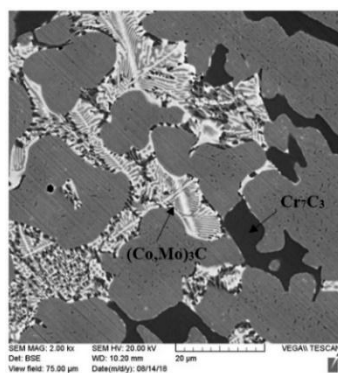
B. Microstructural identification

The microstructures of the alloys were evaluated using a Tescan Scanning Electron Microscope (SEM) with backscatter electron (BSE) imaging to resolve the carbides. To complement the BSE analysis, the SEM is fitted with an energy dispersive X-ray spectroscopy (EDX) unit to qualitatively analyze the different phases by showing the elements present at each selected site for analysis. In addition, X-ray diffraction (XRD) was used to complement the SEM/EDX analysis to accurately identify phases.

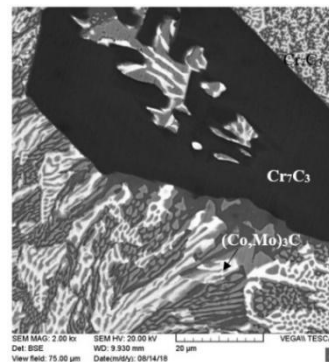
The microstructural analysis shows various phases present in the alloys. However, in general, the three alloys have a microstructure consisting of Cr-rich and Mo-rich carbides embedded in Co solid solution matrix, depending on the Mo content, the amount of Mo-rich carbides varies among the alloys, as shown in Fig. 1. The XRD analysis further identifies Cr₇C₃ carbide (black) and (Co,Mo)₃C carbide (white) present in the alloys, but minor intermetallic compounds are also detected in the microstructures of these alloys. For Stellite 706, there are major dendritic Cr₇C₃ carbide and minor (Co,Mo)₃C carbide distributed across the solid solution matrix, see Fig. 1(a). For Stellite 712, with the increase in C and Mo contents, the amount of Cr₇C₃ and (Co,Mo)₃C carbide apparently increases, as seen Fig. 1(b). Further increased C and Mo contents result in significant increase in (Co,Mo)₃C carbides, along with the augment of primary Cr₇C₃ carbides size, as seen in Fig. 1(c) for Stellite 720.



(a)



(b)



(c)

Fig. 1 SEM microstructure of cast (a) Stellite 706, (b) Stellite 712, (c) Stellite 720

The volume fractions of each phase in the microstructures of the alloy specimens were estimated using SEM and the associated software. The results are reported in Table 2. Stellite 706 has the least amounts of C and Mo among the three alloys, hence its carbide volume fraction is the least. With Stellite 712 and Stellite 720 having more C, more carbides are formed in these alloys. Stellite 720 contains approximately 18 wt.% Mo so that it has the highest volume fraction of Mo-rich carbides.

Table 2: Volume fractions (%) of each phase in the 700 series Stellite alloys

Alloy	Co solid solution	Cr-rich carbide	Mo-rich carbide
Stellite 706	83.45	13.91	2.64
Stellite 712	70.36	24.26	5.38
Stellite 720	55.31	25.09	19.6

C. Hardness and wear tests

The hardness of the alloys was determined on a Wilson Series 2000 Rockwell Hardness Tester. Five tests were performed on each alloy specimen and the average value was taken as the hardness of the alloy. Wear testing was conducted on the Stellite alloys using a NEO-PLUS, NEO-TRIBO Model MPW110 Pin-on-Disc Tribometer in dry-sliding mode, in accordance with ASTM G99–17 Standard Test Method for Wear Testing with a Pin-on-Disc Apparatus [14]. The particular method employed from this standard incorporates a ball mounted in a holder (pin section) which sits directly on top of a disc (specimen). During the test the pin (ball) was pressed under a normal force of 25 N on the specimen and the ball was spinning at a constant rotational speed of 350 rpm. As a result of friction/wear, a 3 mm diameter wear track was generated in the specimen surface, as shown in Fig. 2. The pin is a 5 mm diameter ball, made of tungsten carbide (WC 95 wt.%) and cobalt (5 wt.%). The hardness of the ball material is about 1500HV. The disc specimen dimension is 20 × 20 × 6 mm. The test durations were 1 hr, 3 hr and 5 hr. A CONTOURECORD 1700SD surface texture was utilized to simulate the cross-section profile of the wear track so that the wear loss of the specimen can be quantified. Four locations on each wear track were selected to simulate the cross-section profile. Four tests were performed on each specimen and the wear resistance of the material was evaluated by determining the wear loss which was the volume of the wear track. It can be calculated as the area of the cross-section profile multiplied by the periphery of the wear track.

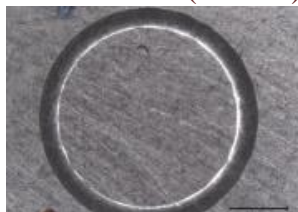


Fig. 2: Wear track generated in the Stellite 720 specimen surface due to dry-sliding wear

D. Electrochemical and immersion corrosion tests

The corrosion performance of the alloys was evaluated using electrochemical and immersion methods. The electrolyte was Green Death solution (11.5% H₂SO₄ + 1.2% HCl + 1% FeCl₃ + 1% CuCl₂), which is a typical industry corrosive environment. ASTM G5-14e1 Standard Reference Test Method for Making Potentiodynamic Anodic Polarization Measurements [15] and ASTM G3-14 Standard Practice for Conventions Applicable to Electrochemical Measurements in Corrosion Testing [16] were followed as the instructions for conducting the polarization tests. The corrosion cell was approximately a 1-liter flat bottom glass flask, which was a three-electrode cell, including a working electrode (WE), a counter electrode (CE) and a reference electrode (RE). The WE was the tested material, which was 16 mm in diameter and 1.6 mm in thickness, mounted on a Teflon holder with a 12 mm diameter surface exposed to the electrolyte. The CE was used to close the current circuit in order to balance the charge added in or removed from the WE. The CE (graphite) did not participate in the electrochemical reactions. The RE (mercury) was used as a control medium to accurately measure and control the WE potential. For both potentiodynamic and potentiostatic experiments, an instrument called Solartron SI 1287 Electrochemical Interface was used. The Solartron provided direct current (DC) for the polarization experiments and the software utilized to extract data is called CorrWare (version 3.2c) and CorrView (version 3.2d). Before starting any specific test, the electrolyte solution was purged with argon gas for 20 min at approximately 1.5 psi pressure, in order to push the air out of the free surface and minimize dissolved oxygen concentration in the solution. Then open circuit potential (OCP) was conducted for about 1.5 hr to achieve an approximately steady-state in order to obtain accurate results. The scan rate for all polarization tests was set to 0.1667 mV/s.

III. RESULTS AND DISCUSSION

A. Hardness and wear loss

The hardness of Stellite 706, Stellite 712 and Stellite 720 was measured to be HRC40, HRC52 and HRC63, respectively. The wear track cross-section profiles are shown in Fig. 3 and the wear losses in volume along with the standard deviations representing the testing errors are illustrated in Fig. 4. It is evident that the wear track in the Stellite 706 surface is the deepest and widest while that in the Stellite 720 surface is the shallowest and narrowest, according to the cross-section profiles of the wear tracks in Fig. 3. Consistently, the former has the largest wear loss and the latter has the least, as illustrated in Fig. 4. For Stellite 720 the wear loss increases with testing (sliding wear) duration, but for Stellite 706 and Stellite 712 longer time (5 hr) wear seems not increasing the wear loss, on the contrary, the wear loss decreases slightly. It is also noticed that the difference in wear loss between the alloys is more apparent for longer time (3 hr

and 5 hr) wear.

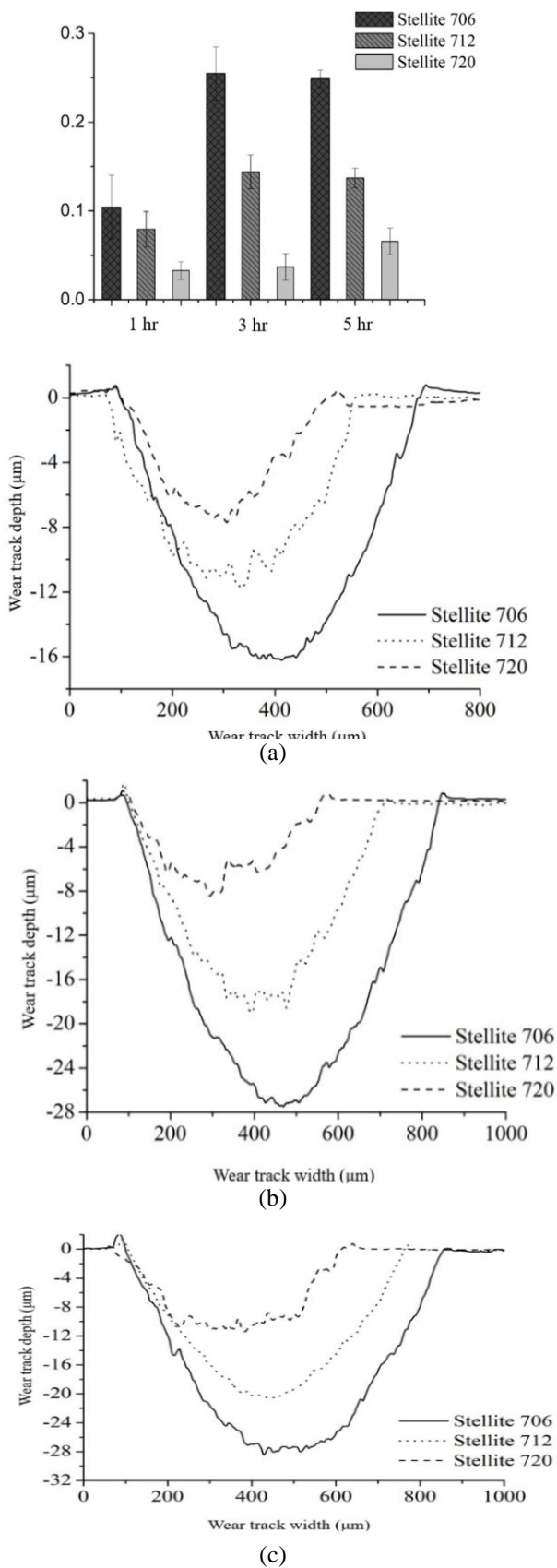


Fig. 3 Cross-section profile of wear track generated in specimen surface tested for (a) 1 hr, (b) 3 hr, (c) 5 hr

Fig. 4 Wear loss from dry-sliding wear test

The worn surface morphologies of the alloys from SEM are shown in Fig.5. The Stellite 706 and Stellite 712 worn surfaces show both abrasive wear and adhesive wear characteristics, with obvious scoring and ploughing as well as an accumulated build-up of plastically deformed particles from the cyclic mechanical attack. During the wear, even at room temperature, friction heat was generated at the contact surface along the wear track. This localized heat generation would cause high temperature oxidation at the ball/disc interface. Stellite alloys are expected to oxidize and the ‘charged’ layer is the oxidized layer (wear debris) lying on the metal surface. Stellite 720 appears to show a significant amount of oxide layer driven features. Very little ploughing and scoring of the surface could be identified. A fine network of cracks developed in the oxide layer and some particles spalled off into the wear path, which indicates that the oxide layer is relatively tough in terms of its adherence to the surface.

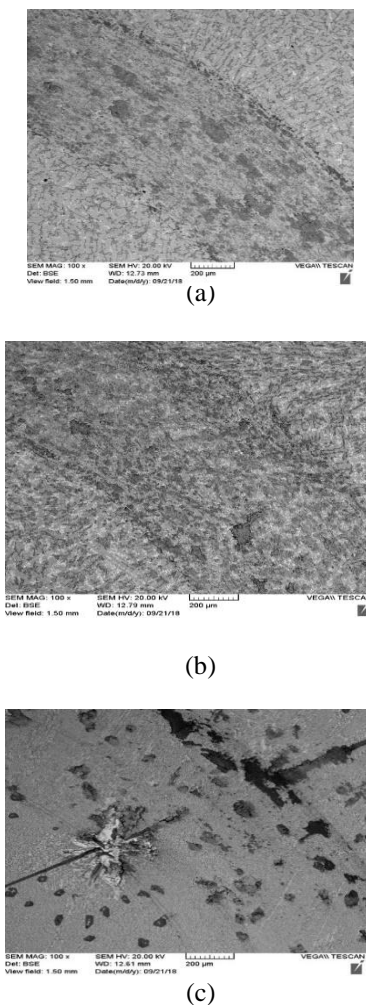


Fig. 5 Worn surface of (a) Stellite 706, (b) Stellite 712, (c) Stellite 720

B. Polarization curve

The potential versus current density curve, also called polarization curve, can be obtained from a polarization test. The important parameters such as corrosion potential E_{corr} , current density I_{corr} , and polarization resistance R_p , which characterize the corrosion behavior of the tested material, can be determined

through analysis of the polarization curve, utilizing the Tafel extrapolation approach [17]. Corrosion potential E_{corr} represents starting of corrosion occurrence on the material. The higher the corrosion potential, the better the corrosion resistance of the material is. Current density I_{corr} is a measure of corrosion intensity of the material. The higher the current density, the more severe the corrosion is. Polarization resistance R_p means the resistance of the material to corrosion. The larger the value of polarization resistance, the more resistant to the corrosive environment the material is.

The potentiodynamic polarization curves of the alloys tested in Green Dath solution are presented in Fig. 6. Visibly the three alloys behave similarly in this medium and the typical characteristic is that these alloys all have an obvious passivation region on the polarization curve, indicating a protective oxide film formed on the specimen surface. However, with continuously increasing the potential, the oxide film can break, characterized by a sudden increase in current. On the other hand, the oxide film exhibits good self-repair capacity, as demonstrated by the tendency of the second passivation on the polarization curves. For detailed results, the calculated values of corrosion parameters from the polarization curves are summarized in Table 3. According to the E_{corr} , I_{corr} and R_p values, Stellite 706 has better anticorrosion performance in resisting electron transferring in the electrochemical reaction, compared to the other two.

The cyclic polarization curve has an additional hysteresis loop because of the reverse scan. If the hysteresis loop is electropositive, that is, the current density of the backward scan is smaller than that of the forward scan at the same potential, the tested material exhibits good localized corrosion (pitting) resistance, whereas if the hysteresis loop is electronegative, the larger the offset, the worse the localized corrosion resistance of the material is [18]. The cyclic polarization curves of the tested alloys in Green Dath solution are presented in Fig. 7. From the reverse scan curves of these alloys, a stable hysteresis behavior is observed as the reverse scan is either close or overlaps the forward scan. This is attributed to the good stability mechanism of the oxide layer on the specimen surfaces as the potential became more positive and swept backward. With a stable hysteresis behavior, these Stellite alloys have extremely small susceptibility to pitting in Green Dath solution.

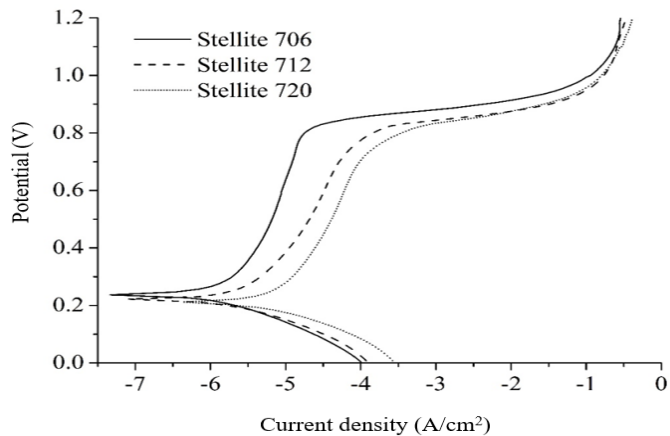


Fig. 6 Potentiodynamic polarization curves of the alloys tested in Green Dath solution

Table 3 Polarization parameters for the alloys tested in Green Death solution

Alloy	E_{corr} (VSCE)	I_{corr} (nA/cm ²)	R_p (kΩ·cm ²)
Stellite 706	0.24	113.78	22.928
Stellite 712	0.22	217.98	11.968
Stellite 720	0.21	450.93	5.785

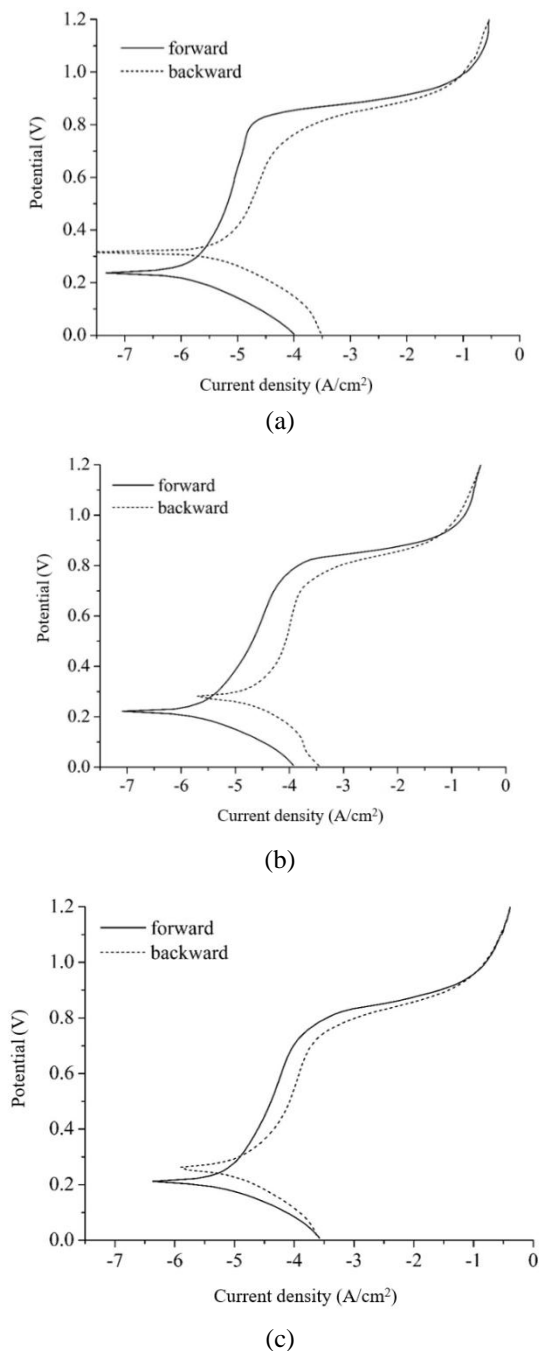


Fig. 7 Cyclic polarization curve of (a) Stellite 706, (b) Stellite 712, (c) Stellite 720 tested in Green Death solution

To better understand the corrosion test results and explore the corrosion mechanism of the 700 series Stellite alloys, the specimen surfaces after the corrosion tests were examined using SEM. It was found that the specimen surfaces after the polarization tests did not show any change. Then the specimens were further immersed in Green Death solution at 60°C for six days to create a more severe corrosive environment. The SEM images of the specimen surfaces after the immersion tests are

presented in Fig. 8. It can be seen that even in this severe corrosive condition the surfaces of the three alloy specimens did not have obvious change, in particular, no pits are observed in the surfaces. In the high-magnification images, the microstructures of the alloys are clearly identified with different phases by etching of the Green Death solution. This also implies that the oxide film had been totally removed from the specimen surface for all the alloys in this testing condition — immersion in Death solution at 60°C for six days.

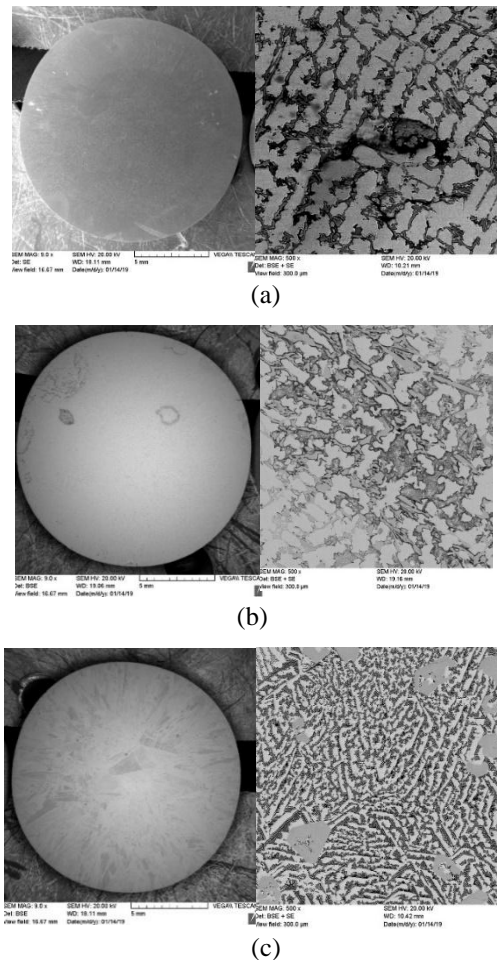


Fig. 8 SEM surface morphology of (a) Stellite 706, (b) Stellite 712, (c) Stellite 720 after 6 day immersion test in Green Death solution at 60°C.

C. Discussion

Different from traditional Stellite alloys, high-C 700 series Stellite alloys — Stellite 706, Stellite 712 and Stellite 720, have a microstructure consisting of both Cr-rich and Mo-rich carbides distributed in Co solid solution matrix due to high Mo and C contents. These carbides benefit the wear resistance of the alloys. The carbide volume fraction data in Table 2 and the wear loss data in Fig. 4 delineate that wear resistance increases with total carbide volume fraction for these alloys. This is because the carbides present strengthen the solution matrix thus reducing plastic deformation in wear. On the other hand, the more the carbides formed, the harder the alloy. It is generally acceptable that the harder the material, the higher the wear resistance is. Stellite 720, with the largest volume fraction of carbides, has the best wear resistance, while Stellite 706, having the least volume fraction of carbides, has the highest wear loss. From the wear

tests, in general, the wear loss increases with sliding time, but for Stellite 706 and Stellite 712, slight reduction in wear loss was observed from 3 hr to 5 hr. There are two possible mechanisms for this occurrence. Compared with Stellite 720, the other two alloys have less carbides thus more solid solution. With continuous wearing, the solid solution could be strengthened by strain-hardening, resulting in less wear. On the other hand, longer sliding promoted oxide formation due to friction heat, which led to the volume increase of the surface layer.

Comparing the performance between CoCrMo and CoCrW system both containing high C content, the former seems not so good as the latter with respect to wear. For instance, W-containing Stellite 6 (29%Cr, 4.5%W, 1.5%Mo, 1.2%C, in weight) and Mo-containing Stellite 706 have the same C content (1.2 wt.%) thus having nearly same carbide volume fraction (~16%), but Stellite 6 is better than Stellite 706 in dry-sliding wear resistance by approximately 1.5 times [13]. This implies that W-rich carbide is more resistant to wear than Mo-rich carbide in Stellite alloys. However, regarding corrosion resistance, high-C CoCrMo system is much better than high-C CoCrW system. As compared with wrought Stellite 6B (30%Cr, 4%W, 1.5%Mo, 1%C, in weight) and Stellite 6K (30%Cr, 4.5%W, 1.5%Mo, 1.6%C, in weight) immersed in Green Death solution at 60°C for 6 days, under the same testing condition, Stellite 706, Stellite 712 and Stellite 720 surfaces almost did not change, at least no pits were observed (Fig. 8), whereas obvious pits were found in the surfaces of W-containing Stellite 6B and Stellite 6K, as shown in Fig. 9. This indicates that high-C CoCrMo system is much better than high-C CoCrW system in corrosion resistance, thus for the applications where wear and corrosion concur, in particular, when the wear and corrosion are severe, the former is superior to the latter. The cyclic polarization curves of Stellite 706, Stellite 712 and Stellite 720 (Fig. 7) agree well with the observations on the specimen surfaces (Fig. 8). With a stable hysteresis behavior, these alloys have extremely small susceptibility to pitting in Green Death solution.



Fig. 9 Pits generated on the surface of (a) Stellite 6B, (b) Stellite 6K after 6 day immersion in Green Death solution at 60°C.

The difference in chemical composition between CoCrW and CoCrMo systems is that the former contains W and the latter contains Mo. The corrosion tests in the present research implied the beneficial effect of Mo on the pitting-corrosion resistance of Stellite alloys. In corrosive media, if the specimen surface is fully covered by a passive film, pitting will not occur. However, if the passive film is damaged or locally broken, then the small region with naked metal becomes anode with the rest region of the surface being cathode, which expedites the anodic oxidation, resulting in pits [17]. Previous research revealed that additional Mo in stainless steels could improve the general and localized

(pitting) corrosion resistance of them within the active regime, such as grain boundaries, pitting zones and cracked oxide areas [19]. The beneficial effect of Mo on the passive properties of stainless steels was attributed to its versatile chemistry in the formation of chlorides and chloride-containing complexes [20]. The presence of Mo in Fe-Cr alloys can lead to the formation of an insoluble salt film on the bottom of the pit. Some Mo chloride salts have a low solubility in aqueous solutions, whereas Fe and Cr chlorides are soluble. Formation of stable chloride complexes may decrease the concentration of free chloride ions within the pit enough to allow repassivation to occur [21]. It was also reported that with the content of Mo up to 28 wt.%, Stellite alloys exhibited significantly improved resistance to non-oxidized acids [22]. Therefore, it is necessary to raise Mo content in the Stellite alloys which are designed for severe corrosive environment applications.

As concerns the three 700 series Stellite alloys being studied, Stellite 706 has the least Mo and C contents, Stellite 720 has the most, and Stellite 712 is in the middle. The C content in Stellite alloys governs the amount of carbides precipitated thus also determines the volume fraction ratio of carbides to solid solution. Since the Cr_2O_3 film formed on Stellite alloys, which has protective effect on the substrate corrosion, results from the oxidation of Cr solute in the solid solution, larger percentage of solid solution would result in larger area of Cr_2O_3 on the alloy surface. Stellite 706 has less carbides thus more solid solution. This means that this alloy would have better oxide film. However, Stellite 706 has less Mo, thus this alloy is worse with respect to the beneficial effect of Mo on repassivation, compared with the other two alloys. The opposite discussion can be made on Stellite 720. Therefore, the corrosion resistance of 700 series Stellite alloys is affected by both C and Mo contents when Cr content is the same. In Green Death solution, Stellite 706 exhibited the best corrosion resistance under polarization among the three alloys, which implied that the amount of Cr_2O_3 film formed played more important role than Mo repassivation effect.

CONCLUSIONS

High-C 700 series Stellite alloys contain Mo varying from 5 to 18 wt.%. Both C and Mo contents influence the microstructure of these alloys significantly. The former determines whether the alloy is hypoeutectic or hypereutectic and also governs the volume fraction of carbides in the alloy, the latter governs the amount of Mo-rich carbides precipitated in the alloy.

The volume fraction of carbides is proportional to the C content in these alloys. The wear resistance of the alloy increases with the carbide volume fraction in the alloy. However, with the same or similar C content, CoCrMoStellite alloy exhibits worse wear resistance than CoCrWStellite alloy.

High-C 700 series Stellite alloys exhibit excellent corrosion resistance without noticeable pitting in Green Death solution, owing to high Mo content. The corrosion resistance of these alloys depends strongly on the behavior of the passivation film formed on the alloy surfaces, which is influenced by both C and Mo contents in addition to Cr content in the alloys. Stellite 706, with the lowest C and Mo contents, exhibits the best corrosion resistance in Green Death solution.

Acknowledgement

The authors are grateful for financial support from the

Natural Science & Engineering Research Council of Canada (NSERC), in-kind support from National Research Council Canada (NRC), and both financial and in-kind support of Kennametal Stellite Inc.

References

- [1] Liu, R., Yao, M.X. (2012) High-temperature wear/corrosion resistant Stellite alloys and Triballoy alloys. CRC Handbook on Aerospace and Aeronautical Materials, CRC Press, Taylor & Francis, 151-235.
- [2] Davis, J.R. (2000) Cobalt-base alloys, in: Nickel, Cobalt, and Their Alloys. ASM International, Materials Park, 362-406.
- [3] Boeck, B.A., Sanders, Jr., T.H., Anand, V., Hickl, A.J., Kumar, P. (1985) Relationships between processing, microstructure, and tensile properties of a Co-Cr-Mo alloy. Powdermetallurgy, 28 (2), 1-10.
- [4] Liu, R., Xi, S.Q., Kapoor, S., Wu, X.J. (2010) Investigation of solidification behaviour and associated microstructures of Co-Cr-W and Co-Cr-Mo alloy systems using DSC technique. Journal of materials science, 45 (22), 6225-6234.
- [5] Liu, R., Wu, X.J., Kapoor, S., Yao, M.X., Collier, R. (2015) Effects of temperature on the hardness and wear resistance of high-tungsten Stellite alloys. Metallurgical and materials transactions A, 46 (2), 587-599.
- [6] Kapoor, S., Liu, R., Wu, X.J., Yao, M.X. (2013) Microstructure and wear resistance relations of Stellite alloys. International Journal of advanced material science, 4 (3), 231-248.
- [7] Liu, R., Yao, J.H., Zhang, Q.L., Yao, M.X., Collier, R. (2015) Relations of chemical composition to solidification behavior and associated microstructure of Stellite alloys. Metallography, microstructure, and analysis, 4 (3), 146-157.
- [8] Aizaz, A., Kumar, P. (1985) Properties of Stellite alloy No. 21 made via pliable powder technology. Metal powder report, 40 (9), 507-510.
- [9] Liu, R., Yao, J.H., Zhang, Q.L., Yao, M.X., Collier, R. (2015) Effects of molybdenum content on the wear/erosion and corrosion performance of low-carbon Stellite alloys. Materials and design, 78, 95-106.
- [10] Huang, P., Liu, R., Wu, X.J., Yao, M.X. (2007) Effects of molybdenum content and heat treatment on mechanical and tribological properties of a low-carbon Stellite alloy. Journal of engineering materials and technology, 129 (4), 523-529.
- [11] Yao, J.H., Ding, Y.P., Liu, R., Zhang, Q.L., Wang, L. (2018) Wear and corrosion performance of laser-clad low-carbon high molybdenum Stellite alloys. Optics and laser technology, 107, 32-45.
- [12] Hu, P.S., Liu, R., Liu, J., McRae, G. (2014) Investigation of wear and corrosion of a high-carbon Stellite alloy for hip implants. Journal of materials engineering and performance, 23 (4), 1223-1230.
- [13] Liu, R., Yao, J.H., Zhang, Q.L., Yao, M.X., Collier, R. (2015) Microstructures and hardness/wear performance of high-carbon Stellite alloys containing molybdenum. Metallurgical and materials transactions A, 46 (12), 5504-5513.
- [14] [14] ASTM G99-17 (2017) Standard Test Method for Wear Testing with a Pin-on-Disk Apparatus, American Society for Testing and Materials, West Conshohocken, Pennsylvania.
- [15] ASTM G5-14e1 (2014) Standard Reference Test Method for Making Potentiodynamic Anodic Polarization Measurements, American Society for Testing and Materials, West Conshohocken, Pennsylvania.
- [16] ASTM G3-14 (2014) Standard Practice for Conventions Applicable to Electrochemical Measurements in Corrosion Testing, American Society for Testing and Materials, West Conshohocken, Pennsylvania.
- [17] Perez, N. (2004) Kinetics of activation polarization. Electrochemistry and corrosion science, Kluwer Academic Publishers, Assinippi Park, 71-120.
- [18] Kelly, R.G., Scully, J.R., Shoesmith, D., Buchheit, R.G. (2002) Passivity and localized corrosion. Electrochemical techniques in corrosion science and engineering, 18, Narceck Dekker, Inc., New York, 44-55.
- [19] Bastidas, J.M., Torres, C.L., Cano, E., Polo, J.L. (2002) Influence of molybdenum on passivation of polarized stainless steels in a chloride environment. Corrosion science, 44 (3), 625-633.
- [20] Olefjord, I., Brox, B., Jelvestam, U. (1985) Surface composition of stainless steels during anodic dissolution and passivation studied by ESCA. Journal of the electrochemical society, 132 (12), 2854-2861.
- [21] Olefjord, I., Fischmeister, H. (1975) ESCA studies of the composition profile of low temperature oxide formed on chromium steels — II. corrosion in oxygenated water. Corrosion science, 15 (6-12), 697-707.
- [22] Sims, C.T. (1969) A contemporary view of cobalt-base alloys. JOM, 21, 27-42.